Peripheral nerve graft architecture affects regeneration

Vleggeert-Lankamp, Carmen Lia Anne-Marie

CHAPTER 6

Biodegradation of a synthetic nerve graft has a moderately beneficial effect on peripheral nerve regeneration

C.L.A.M. Vleggeert-Lankamp[a], J.F.C. Wolfs[a], A.P. Pêgo[b], R.J. van den Berg[c], H.K.P. Feirabend[a], M.J.A. Malessy[a], E.A.J.F. Lakke[a]

[a]Neuroregulation group, Department of Neurosurgery; [c]Department of Neurophysiology, Leiden University Medical Centre (LUMC), Leiden, the Netherlands; [b]Institute for Biomedical Technology (BMTI), Department of Polymer Chemistry and Biomaterials, University of Twente, Enschede, The Netherlands

Abstract

In the present study we analyse the influence of the biodegradability of synthetic nerve grafts on nerve regeneration. Nerve guides with an outer layer of trimethylene carbonate (TMC)/ poly-ε-caprolactone (CL) and an inner layer of either TMC/CL (*fast degradable* graft) or TMC (*slowly degradable* graft) were compared to each other, and to autografts and unoperated nerves. Twelve weeks after bridging a 6 mm sciatic nerve lesion in the rat, the integrity of the nerve guides, the morphology of nerve at midgraft, morphometrical parameters of nerve and innervated muscle, and electrophysiological parameters of the nerve were evaluated. Based on the observed changes of the number and diameter of the regenerated nerve fibres predicted values of the electrophysiological parameters were calculated, to be compared to the actually measured values.

This study shows that the *fast degradable* graft disintegrated and that the *slowly degradable* graft remained partially intact. The values of the morphometrical parameters of the peroneal nerves and the gastrocnemic and tibial muscles were similar if not equal in the synthetic nerve grafted rats, while some of the electrophysiological parameters were different. The refractory period in the *fast degradable* nerve grafts was equal to unoperated nerves, while it lenghtened in *slowly degradable* nerve grafts. In both *slow* and *fast degradable* nerve grafts the conducted charge diminished, and in *slowly degradable* grafts the charge even fell below the expected value. Though the observed differences are small, *fast degradable* grafts are preferred over *slowly degradable* grafts.

Introduction

Nerve regeneration studies following implantation of newly developed synthetic nerve grafts appear on a regular base (see [1-9] for reviews). In general, the quality of regeneration through a novel device is evaluated by comparison to unoperated or autografted nerves and the purport of the conclusion is whether that specific device should be used in future studies or even in a clinical setting or not. Studies designed to assess the aptness of certain graft properties (biodegradability, porosity, surface wettability, surface microgeometry etc) in general, i.e. as independent from specific nerve grafts as possible, would allow to define which properties are desirable, which not. This in turn would allow to formulate the strategy for the development of an artificial nerve graft in a much more rational way.

In the present study we consider the relationship between biodegradability of a nerve graft and regeneration. Studies comparing *fast* to *slowly degradable* grafts with the specific aim to investigate the effect of degradability on nerve regeneration are scarce [10-12, 13-18], and inconclusive. Ambiguous results were obtained due to the failure to demonstrate the biodegradability of the nerve graft under study [11, 12, 14, 17], due to the choice of the evaluation method [13, 15, 16, 19], and due to the fact that the effects of porosity and biodegradability were not always distinguished properly [10]. Nevertheless differences in degradability were unequivocally correlated to differences in number and size of the regenerated axons in at least one study [18], apparently attesting to the desirability of degradability. It has been demonstrated, however, that larger numbers of regenerated nerve fibres not neccesarily correlate to a better electrophysiological function [20] or to improved muscle morphology [21].

A potential biomaterial to construct a new synthetic nerve graft is trimethylene carbonate (TMC) [22-25]. TMC is flexible, strong and undergoes slow degradation *in vivo* to non-toxic products [26, 27]. TMC can be combined with poly-ε-caprolactone (CL) resulting in a copolymer with a lower molecular weight than TMC or CL homopolymers [28]. The degradation of the copolymer increases with a lower molecular weight [29], and it has indeed been demonstrated that TMC/CL (10:90) degrades faster than TMC *in vitro* [30].

In this study, microporous nerve guides with an outer layer of TMC/CL and an inner layer of either TMC/CL (*fast degradable* graft) or TMC (*slowly degradable* graft) were compared to each other, and to autografts and unoperated nerves. Twelve weeks after bridging a 6 mm sciatic nerve lesion in the rat, the integrity of the nerve guides, the morphology of nerve at midgraft, morphometrical parameters of nerve and dependent muscle, and electrophysiological parameters of the nerve were evaluated. Based on the observed changes of the number and diameter of the regenerated nerve fibres predicted values of the electrophysiological parameters were calculated, to be compared to the actually measured values. The goal was to analyse whether the degradation of a synthetic nerve graft effects peripheral nerve regeneration, i.e. to assess the desirability of (bio)degradation.

Materials and methods

Synthetic nerve graft preparation

We implanted hollow synthetic nerve grafts consisting of two layers. The inner layer was fabricated by a dipcoating technique and consisted of porous TMC (referred to as '*slowly degradable* graft') or porous TMC/CL (10:90) (referred to as '*fast degradable* graft'). To introduce micropores in the inner layer sugar crystals (<20 µm) were added, which were later allowed to leach out. The macroporous outer layer was nearly similar in both grafts and consisted of TMC/CL that was spun around the inner layer (fig. 1). The preparation of these tubes was

Figure 1: Synthetic nerve grafts

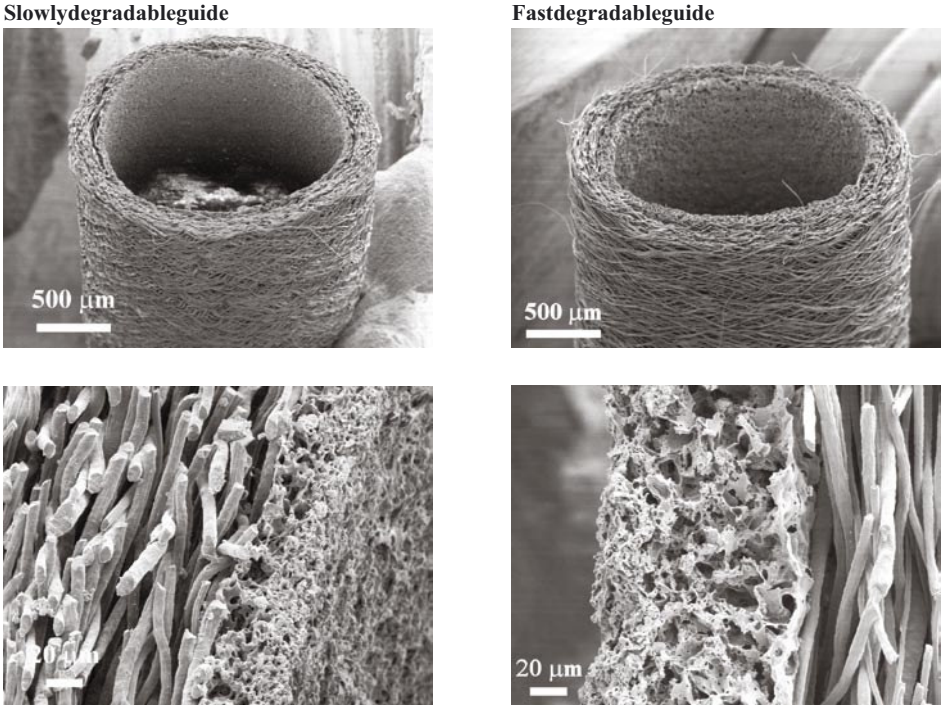

Scanning electron micrographs of cross-sections and details of the two-layer connections of *slowly* and *fast degradable* grafts. SEM analyses were carried out using a Hitachi S800 field emission scanning electron microscope at voltages of 3-5 kV [32].

Table 1: Characterization of synthetic tubes

			Wall thickness (µm)		**Pore size** (µm)	
	TMC/CL ratio in outer layer	**inner diameter** (mm)	inner layer	outer layer	inner layer	outer layer
Slowly degradable graft	11 : 89	1.5	30	179	1-13	15-80
Fast degradable graft	10 : 90	1.7	92	161	3-58	50-150

Internal diameter, wall thickness and porosities of the inner and outer layer of *slowly degradable* and *fast degradable* tubes, examined by scanning electron micrography (SEM).

comprehensively described in previous studies [31, 32]. The physical properties of the resulting tubes were specified in table 1. All tubes had good flexing characteristics, and bending caused only a small reduction of the cross-sectional area of the tubal lumen.

In liquid nitrogen, tubes were cut into nerve grafts of 10 mm length. Prior to implantation, the nerve grafts were sterilized by rinsing them for 10 seconds in a 70 vol% ethanol solution, followed by a thorough rinse in sterilized water.

Animal model

A total of 30 female Wistar rats (HsdCpb:WU), weighing 220-240 grams, were used for this study. Rats were housed in flat bottomed cages in a central animal-care facility, and maintained on a 12-hour light cycle regime at a controlled temperature of 22°C. Standard rat chow and water were available *ad libitum*. Animals were randomly assigned to the control or to one of four sciatic nerve repair groups. Both sciatic nerves of 6 unoperated rats served as controls, 12 rats received an autograft, 6 rats received a *slowly degradable* graft, and 6 rats received a *fast degradable* graft. All grafting experiments were performed on the left sciatic nerve. Muscles reinnervated by an autografted nerve will be referred to as 'autograft muscles', and peroneal nerves distal to an autograft will be referred to as 'autograft peroneal nerves'. A similar nomenclature will be used for the muscles reinnervated by synthetic grafted nerves, and peroneal nerves distal to synthetic nerve grafts (for instance '*slowly degradable* graft muscle' and '*slowly degradable* graft peroneal nerve'). All experiments were performed in accordance with international and local laws governing the protection of animals used for experimental purposes (UDEC 99105).

Surgical procedures

For the grafting procedure, rats were given general inhalation anesthesia of isoflurane in a 1:1 mixture of O_2 and N_2O. To improve anesthesia and to diminish post-operative pain, buprenorphine (0.1 ml of 0.3 mg/ml; Temgesic®, Schering-Plough, Maarssen, the Netherlands) was injected intraperitoneally. Microsurgical dissection was performed with the aid of a Zeiss operating microscope under aseptic conditions. All animals were operated on in the same time span by the same surgeon. The left sciatic nerve was exposed and isolated at the midthigh level via a dorsal approach. In rats receiving an autograft, a 6 mm nerve segment was resected. The nerve segment (autograft) was reversed longitudinally and grafted into the gap with 4 epineurial sutures (10-0 monofilament nylon) at each end. In rats receiving a synthetic nerve graft, a 2 mm nerve segment was resected. The proximal and distal nerve stump were inserted into the synthetic nerve graft, leaving an interstump distance of 6 mm. Fibrin glue (Tissucol®, Baxter, Vienna, Austria) was used to affix the nerve stumps in the graft. The wound was closed in layers. After a post-operative survival period of 12 weeks, the rats were anaesthetized as described above, and the left sciatic nerve was exposed at the midthigh level via a dorsal approach. The (grafted) sciatic nerve was inspected, resected and stored in an electrolyte solution (140 mM NaCl, 3.0 mM KCl, 1.5 mM $CaCl_2$, 1.25 mM $MgSO_4$, and 11.0

mM glucose in 5.0 mM Tris buffer, pH 7.4, 20 °C). Immediately following resection of the sciatic nerves, the gastrocnemic and anterior tibial muscles were exposed, resected, embedded in Tissuetek® (Sakura, Zoeterwoude, the Netherlands), rapidly frozen in liquid nitrogen cooled isopentane [33], and stored at -80°C. Finally the animals were euthanized.

Midgraft nerve morphological analysis

The amenability of each graft type to the formation of a tissue bridge between the nerve stumps, a prerequisite for nerve regeneration, was gauged by scoring the presence of such a bridge in each case. After the electrophysiological recordings were performed (see below), the nerve was stored in 4% formaldehyde solution (0.1 M phosphate buffered at pH 7.2) for at least a few weeks. Subsequently, 4 mm long samples were resected from the middle of the graft for microscopic inspection. Upon dehydration in ascending series of ethanol, the tissue samples were embedded in paraffin (Klinipath, Duiven, The Netherlands). Transverse 4 µm sections were cut and alternatingly stained for general appearance (haematoxylin/eosin), for myelin (Klüver-Barrera [34]), and for collagen (Verhoef van Gieson [35]).

The following criteria were applied to adjudge whether the graft was considered to be disintegrated:

1. remains of the biomaterial should not be present 'en bloque' but merely as small rem - nants;
2. a capsular structure around the regenerated structure should be absent, or, if present, at least fragmented;
3. the size of the diameter of the regenerated structure should at least be smaller than the inner diameter of the nerve graft

Peroneal morphological analysis

Histology

The preparation of cross-sections of peroneal nerves and the subsequent microscopy and im - age analysis was comprehensively described in previous studies [20, 21]. In short, the nerves were immersion fixated and embedded in Epon® (Merck, Amsterdam, The Netherlands). Trans - verse 1 µm sections were stained with a 1% toluidine blue / 1% borax solution [36]. The nerve area, the mean nerve fibre diameter, the fibre density and the total number of nerve fibres were determined. Subsequently, the diameters of the nerve fibres were distributed into 180 classes of 0.1 µm each, and plotted against the percentage of the number of fibres present in that class. By fitting the sum of two lognormal functions to the frequency distributions of fibre diameters, the mean diameter and the number of fibres for the separate Aα- and Aβ-fibre populations were exposed. Fittings to two lognormal functions was compared to fittings with a single lognormal function using Akaike's Information Criterium (AIC).

Muscle morphological analysis

Immediately following the resection of the sciatic nerves, the gastrocnemic and anterior tibial muscles were exposed, resected, embedded, cut in 10 µm thick cross sections, and stained for myofibrillar ATPase. Microscopic video images of the sections were taken and the muscle cross sectional area (muscle CSA), the number of type I and type II muscle fibres, and the fibre cross sectional area of the type I and type II muscle fibres was determined as described elsewhere [21].

Electrophysiological evaluation

The *in vitro* electrophysiological evaluation of the sciatic nerve, including the peroneal and tibial nerve, was comprehensively described in a previous study [20]. In short, the resected nerve was mounted on a moist chamber filled with an electrolyte solution (see above) in such a way that the grafted part was entirely floating in the middle pool. The nerve fibres were progressively recruited by extra-cellular excitation, while the propagated monophasic action potentials were measured and normalized in terms of compound action currents [20].

The presence *per se* of a measurable electrophysiological response was registered, and expressed as the *response rate*. When a response was present, then the displaced electrical charge was calculated (Q). Q_{max} was defined as the area under the curve of the maximum action current. The other parameters calculated were the mean conduction velocity (MCV), the mean voltage threshold (V_{50}), and the mean refractory period (t_{50}). In the absence of a measurable electrophysiological response, Q_{max} was considered 0, and MCV, V_{50} and t_{50} remained undetermined.

In order to discriminate the Aα- and Aβ-fibre populations, two *erf*-functions were fitted to the stimulus-recruitment and interpulse time-recruitment curves [20]. Consequently values for $Q_{max,\alpha}$, $Q_{max,\beta}$ (calculated from stimulus-recruitment and interpulse time-recruitment curves separately), $V_{50,\alpha}$, $V_{50,\beta}$, $t_{50,\alpha}$ and $t_{50,\beta}$ could be obtained.

Again, to evaluate the validity of fitting with two instead of one *erf*-function, AIC was used.

Prediction of firing threshold and refractory period based on diameter of nerve fibres

In the normal nerve there exists an empirical inverse relation between the diameter of the nerve fibres and both the extracellular firing threshold [37, 38] and the refractory period [39]. This relation can be exploited to assess qualities of the regenerated nerve fibres. Based on the observed mean diameter in the experimental groups and the mean diameter and mean voltage threshold of the control group the predicted values of the mean voltage threshold in the experimental group can be calculated using equation 1

$$V_{50,g,predicted} = \frac{V_{50,c} * d_{Fmax,c}}{d_{Fmax,g}} \qquad \text{(eq. 1)}$$

The predicted value of the mean refractory period (eq. 2), as well as the predicted values of the mean thresholds and refractory periods of the Aα- and Aβ-fibre populations can be calculated with the same equations, by substituting the appropriate values.

$$t_{50,g,predicted} = \frac{t_{50,c} * d_{Fmax,c}}{d_{Fmax,g}} \quad \text{(eq. 2)}$$

Prediction of charge displaced based on number and diameter of nerve fibres

The charge, Q_{max} is proportional to the product of the number of excitable nerve fibres and the square of their mean diameter [cf. 20, 40]. Hence the predicted value of Q_{max} can be calculated with equation 3. Predicted values of Q_{max} of the Aα- and Aβ-fibre populations can be calculated with the same equation, by substituting the appropriate values.

$$Q_{max,g,predicted} = \frac{Q_{max,c} * N_g * d^2_{Fmax,g}}{N_c * d^2_{Fmax,c}} \quad \text{(eq. 3)}$$

Comparison of the experimentally measured values of these parameters to the predicted values will yield some insight in the quality of regeneration (see discussion).

Statistical evaluation

The means of all parameters were shown with standard deviations (mean ± sd). Student's t-tests were applied to the means to compare the control and autograft values with the synthetic nerve graft values. If a statistical significant difference was found with two or more of the synthetic nerve graft values, a one-way ANOVA was applied to the means, followed by Tukey's least significant differences multiple comparisons test to investigate differences between the groups. Fisher exact tests were applied to the electrophysiological response rates. Kolmogorov-Smirnow tests were applied to the different nerves and to the different samples per nerve for comparison of size distributions [41, 42]. Paired Student's t-tests were used to compare calculated and predicted values of V_{50}, t_{50} and Q_{max}. The SPSS statistical program, version 11.0, and Origin, version 5.0, were used to calculate means and standard deviations, and to perform statistical analysis. P-values of less than 0.05 or, in case of the electrophysiological-morfometrical relations 0.05 and 0.10, were regarded as significant.

Results

All autografted nerves exhibited a patent graft at 12 weeks after surgery. The grafted part was slightly thinner. The distal nerves proved to be firm and shiny white, without the softening one would expect after Wallerian degeneration [19]. Some connective tissue was present around the coaptation sites.

Upon inspection of the *fast degradable* grafted nerves twelve weeks after surgery, it was obvious that a tissue cable had connected the two nerve stumps, and the site where the nerve

graft was implanted could not be recognized as such. In the group of the *slowly degradable* grafts, the site where the grafts had been implanted was clearly distinguishable because the tube had deformed to a gel-like shell around the tissue cable that connected the two nerve stumps. A tissue bridge was present in all rats in both synthetic nerve graft groups.

Midgraft morphology

In midgraft cross-sections of both types of synthetic nerve grafts a centrally located nerve-like structure was surrounded by a cell-rich outer layer (fig. 2). The nerve-like structure contained myelinated nerve fibres, cell nuclei (at least some of them Schwann cell nuclei since myelin was present around the nerve fibres) and an amorphous extracellular matrix. The outer layer contained circularly oriented fusiform cells (presumably fibroblasts) embedded in an extracel - lular matrix rich in collagen. Thin walled blood vessels and capillaries were observed through - out the cross section, though most of the larger vessels were located in the outer layer. In the *slowly degradable* grafts, throughout the cell-rich layer trabecular structures were present that were most likely to be the remains of the tubal wall. These structures were not present or fragmented in the cell-rich layers of the *fast degradable* grafts. Thus, in the *slowly degradable* nerve grafts, the remains of the tubal wall appeared to be present 'en bloque'. Throughout the cell-rich layer of both *slowly degradable* and *fast degradable* grafts pieces of smooth material surrounded by rings of large round cells could be distinguished. The smooth material made the impression of the remains of biomaterial, broken down by the round large cells.

Figure 2: Light microscopic midgraft cross-sections of regenerating nerves

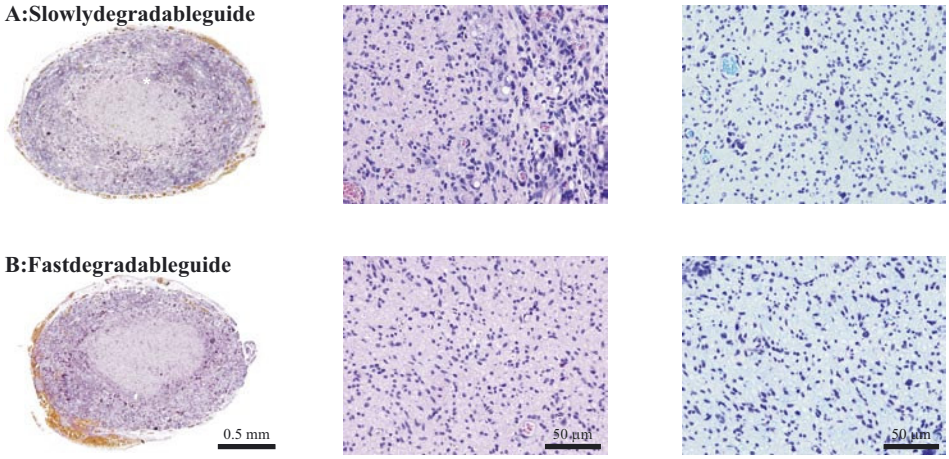

Transverse (4 µm) cross-sections of midgraft sciatic nerves, immersion fixed after electrophysiological evaluation, and stained with haematoxylin/eosin, according to the method of lüver-Barrera to clearly identify myelin sheaths [34], and according to the method of Verhoef van Gieson to clearly identify collagen [35] are depicted. In all figures, the left panel represents the Verhoef van Gieson stained nerve section as a whole. Elastic fibres are stained black, nuclei blue and cytoplasm yellow/ brown. The middle panel represents an enlarged sample of the haematoxylin/eosin nerve section and demonstrates the morphology of the nerve in detail. The right panel depicts an enlarged sample of the nerve section, stained according to the method of Klüver-Barrera, in which the myelin sheath is deep blue and is therefore more pronounced.
A. Cross-section of a *slowly degradable* nerve graft. B. Cross-section of a *fast degradable* nerve graft.

The *slowly degradable* grafts were encapsulated by a continuous structure, which was rich in collagen. This encapsulating structure also contained pieces of smooth material, which remarkably demonstrated to have round large cells in the center, as though breakdown of the biomaterial took place from the inside of the pieces of biomaterial. This encapsulating structure was absent in the *fast degradable* grafts.

The cross-sectional size of the structures that regenerated through the degradable porous grafts was smaller compared to the structures that regenerated through the *slowly degradable* grafts. It was not evident whether this was caused by a smaller central area, a smaller cell-rich area or the absence of an encapsulating structure. In all synthetic nerve grafts, but mainly in the *slowly degradable* grafts, the cross-sectional shape of regenerated structure was oval, as though the grafts were partially squeezed *in vivo*, causing the regenerated nerve cable to adopt this shape.

Morphology of the peroneus

Light microscopy of sections demonstrated that the regenerated peroneal nerves were vascularized and enclosed in a connective-tissue sheath. They contained many myelinated axons, abundant endoneurial connective tissue and blood vessels (fig. 3, left column). The myelin sheaths of the nerve fibres in grafted nerves were thin in comparison to those in controls. The nerve fibres in the autograft peroneal nerve, and to a lesser extent, in the *fast degradable* peroneal nerve, were frequently fasciculated within areas of size comparable to the cross-section of single myelinated fibres in the control nerve, suggesting regeneration of several nerve fibres through single Schwann cell basal laminar scaffolds that persisted after Wallerian degeneration of the original myelinated nerve fibres [43]. The fibre diameter frequency distributions (fig. 3, middle and right column) demonstrated that in regenerating peroneal nerves fibre diameters shifted to smaller sizes.

All nerve areas were of comparable size (fig. 4A), and the fibre diameters of grafted nerves were halved compared to controls (fig. 4B). The total number and the density of nerve fibres were doubled after autografting, and remained unchanged in experimentally grafted nerves (fig. 4C and D).

Kolmogorov-Smirnow tests revealed a homogeneous fibre size distribution throughout control nerves, and a homogeneous fibre size distribution within individual control nerves. In the regenerating nerves, both heterogeneity and homogeneity in fibre size distributions between nerves, and within individual nerves, were encountered.

The sum of two lognormal distributions could satisfactorily be fitted to the fibre diameter distributions of both control and graft peroneal nerves (fig. 3, right column). In all examined nerves, the AIC was determined and shown to be smaller ($p<10^{-4}$) for two populations compared to one, indicating that the fibre diameter distribution could be more aptly described by the sum of two lognormal distributions rather than by one lognormal distribution.

In control peroneal nerves, the number of Aβ-fibres was somewhat higher compared to the number of Aα-fibres (fig. 4E). In regenerated nerves it was the other way round: the number of

Figure 3: Light microscopic cross-sections and frequency distributions of control and graft peroneal nerves

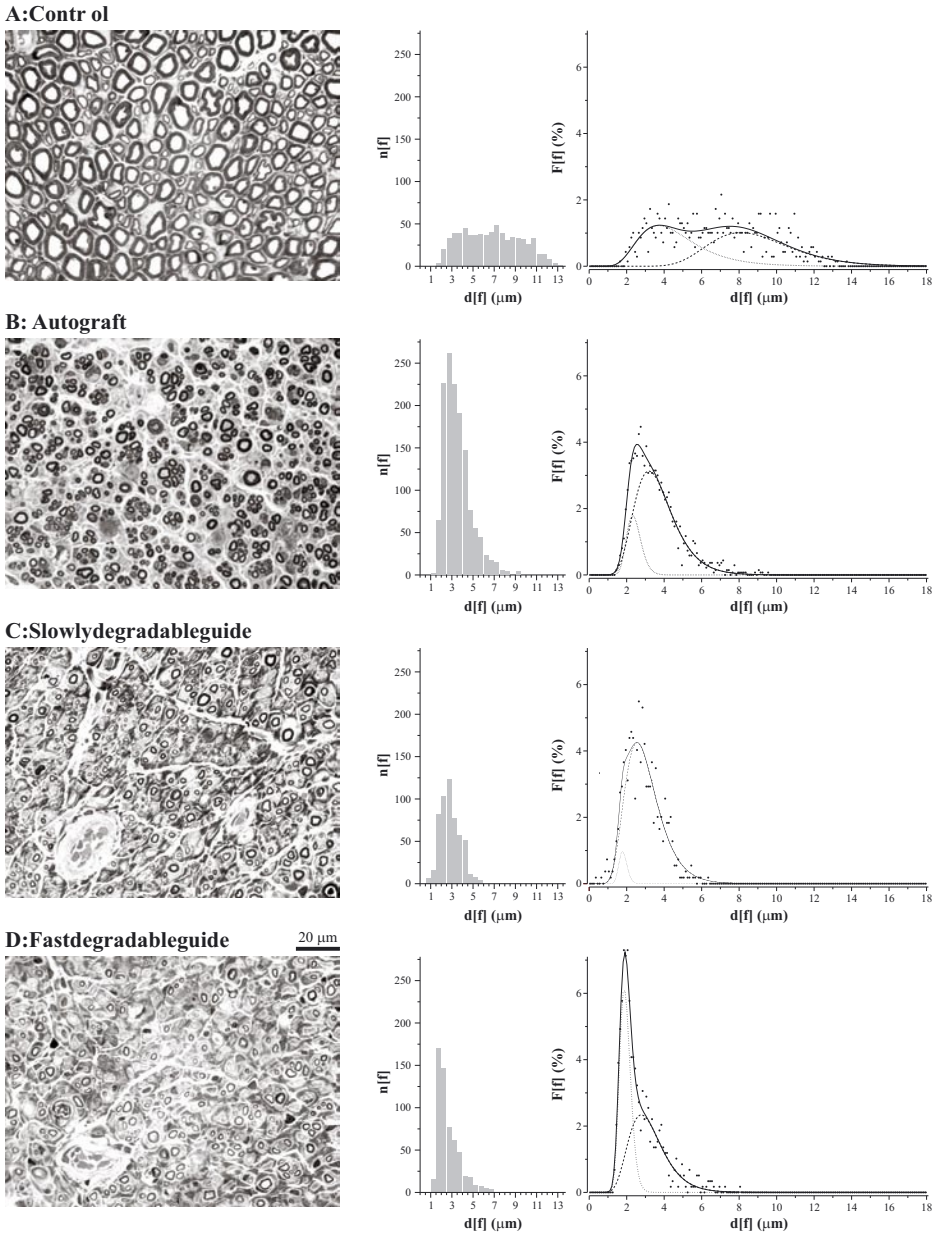

Transverse semi-thin (1 µm) cross-sections of peroneal nerves, immersion fixed after electrophysiological evaluation, and stained with a 1% toluidine blue / 1% borax solution [36] are depicted. In all figures, the left panel represents the nerve section as a whole, whereas in the middle panel an enlarged sample of this nerve section (square) demonstrates the morphology of the nerve in detail. The right panel depicts typical examples of the frequency distributions of fibre diameters of control, autografted, *slowly degradable* and *fast degradable* grafted peroneal nerves. In each graph, diameters of the nerve fibres were distributed into 28 classes of 0.5 µm each, and plotted against the fibre diameter class frequency. The dots represent the calculated fibre diameter class frequency per fibre diameter class, the straight line represents the fit of total curve, the dotted line represents the Aβ-fibre population, and the dashed line represents the Aα-fibre population.

Figure 4: Morphometric analysis

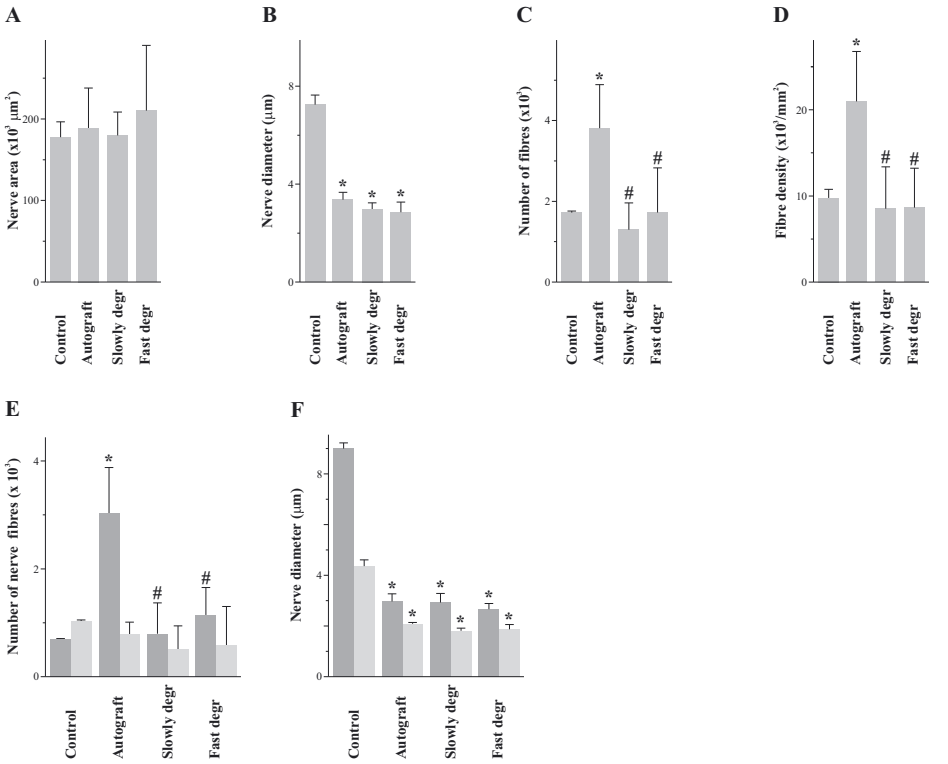

Morphometric data of the control, autografted and synthetic grafted nerves are depicted. Peroneal nerves from the control group were aselectly chosen for evaluation (n = 4). From the autografted (n = 12) and synthetic grafted (n = 6 per group) groups, all peroneal nerves were evaluated. A. The total surface of the nerve cross section (nerve area), B. the nerve fibre diameter, C. the number of nerve fibres, D. the nerve fibre density, E. the number of nerve fibres for the Aα- and Aβ-fibre population separately, and F. the nerve fibre diameter for the Aα- and Aβ-fibre population separately. Data are represented as mean (± sd). (*) Different compared to control nerves. (#) Different compared to autograft nerves.

Aα-fibres was higher than the number of Aβ-fibres. In autograft peroneal nerves, the number of Aα-fibres increased fivefold, while in the synthetic grafted nerves the number of Aα-fibres remained equal. In all regenerated nerves, the number of Aβ-fibres remained unchanged. The diameter of Aα-fibres decreased three times and the diameter of Aβ-fibres halved in all experimental nerve fibres (fig 4F).

Morphology of the muscles

Control tibial and gastrocnemic muscles contained predominantly type II fibres. In the tibial muscle, only 2% of the muscle fibres were type I fibres, and these were dispersed throughout the muscle. In the gastrocnemic muscle, 10% of the muscle fibres were type I fibres, these were predominantly localized in the lateral belly, though some were randomly dispersed through the rest of the muscle. In nerve graft muscles, type II muscle fibres were still predominant in the tibial (95 to 100%) and gastrocnemic (94 to 95%) muscles, but the grouped presence of type I fibres in the lateral belly of the gastrocnemic muscles had disappeared.

Table 2: Muscle CSA and reorganization of type I and type II musclefibres after reinnervation

Tibial muscle	muscle CSA (x 10^6 µm^2)	number of type I muscle fibres	type I muscle fibre CSA (µm^2)	number of type II muscle fibres	type II muscle fibre CSA (µm^2)
Control	38.1 ± 6.5	170 ± 97	1410 ± 256	7774 ± 1154	4883 ± 587
Autograft	22.6 ± 6.5*	314 ± 209	2093 ± 623	6113 ± 1866	3636 ± 721*
Slowly degradable graft	19.2 ± 3.4*	20 ± 4*#	1294 ± 275	7541 ± 1088	2620 ± 673*
Fast degradable graft	22.6 ± 3.0*	80 ± 55	2162 ± 291*	6985 ± 1373	3269 ± 528*
Gastrocnemic muscle	muscle CSA (x 10^6 µm^2)	number of type I muscle fibres	type I muscle fibre CSA (µm^2)	number of type II muscle fibres	type II muscle fibre CSA (µm^2)
Control	73.8 ± 6.4	1256 ± 462	2322 ± 405	11079 ± 1777	6474 ± 520
Autograft	43.2 ± 8.7*	635 ± 397*	3002 ± 703	11459 ± 2720	3700 ± 661*
Slowly degradable graft	32.6 ± 8.7*	451 ± 248*	1427 ± 458*#	10945 ± 1895	3007 ± 974*
Fast degradable graft	38.1 ± 9.7*	445 ± 293*	2229 ± 786	12751 ± 3527	3137 ± 654*

Muscle CSA, type I and type II muscle fibre number and CSA in muscles innervated by control, autografted, *slowly degradable* and *fast degradable* nerve grafted sciatic nerves. Data are represented as mean (± sd). (*) Different compared to control muscles. (#) Different compared to autograft muscles.

One of the *fast degradable* graft tibial muscles was extremely atrophic, and obviously not reinnervated. This muscle was excluded from further evaluation.

The muscle CSA diminished to half its size in grafted muscles (table 2). The type II muscle fibre CSA also declined to half its size in graft muscles, which was not surprising, regarding the predominance of type II muscle fibres. The number of type II muscle fibres remained equal. An overall impression of the changes in type I muscle fibres is that the opposite takes place. Type I muscle fibre CSA remained equal in graft muscles, and only showed an increase in the *fast degradable* graft tibial muscles and a decrease in *slowly degradable* graft gastrocnemic muscles in comparison to control muscles. The number of type I muscle fibres diminished. This was more pronounced in gastrocnemic muscles compared to tibial muscles.

Electrophysiology

In control and autografted nerves, all nerves displayed an electrophysiological response. In the *slowly degradable* group, 4 of 6 cases demonstrated a response, and in the *fast degradable* group all 6 cases displayed a response (figure 5B), which was statistically comparable.

The amplitude of the monophasic action current gradually increased in response to increasing stimulus voltages, until a maximum amplitude was reached (fig. 5A). The voltage stimulus necessary to attain the maximum action current amounted to approximately 4 V in control nerves and 10 V in grafted nerves. Q_{max} was highest in control nerves, lower in autografted nerves, and lowest in the synthetic grafted nerves (fig. 5C and D). Q_{max} of the *slow* and *fast degradable* grafted nerves was equal, and the mean value of Q_{max} derived from the interpulse time-recruitment curves was comparable to that obtained from the stimulus-recruitment curves.

The MCV was three to four times slower in auto- and synthetic grafted nerves, and the differences between grafted nerves were not significant (fig. 5E).

Figure 5: Recordings of compound nerve action currents

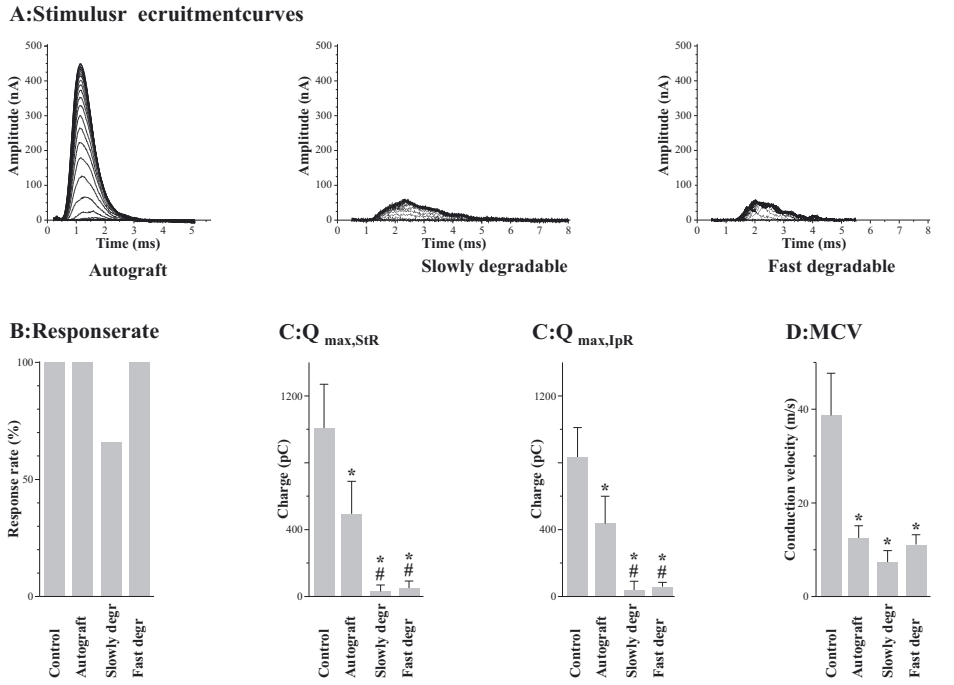

A. Examples of the time courses of compound action currents as a function of stimulus voltage of synthetic grafted sciatic nerves. In each graph, the curves from bottom to top represent compound action currents, evoked by increasing stimulus voltages. Stimulus artifacts were erased. Due to the virtual cathode effect [68] the onset of the current moves closer to the stimulus artifact upon increasing the stimuli. Rundown of the compound action current due to *in vitro* deterioration of the nerve fibres was calculated from the spontaneous decrease of Q_{max} during measurements, and amounted to 4%/hr in control and 10%/hr in autografted nerves. In a pilot experiment with synthetic nerve grafts, we noted that rundown was more pronounced compared to control and autografted nerves, causing the response to deteriorate significantly after approximately five to ten minutes of measuring. In the current experiment the measurements never lasted longer than five minutes.

B. Electrophysiological response rate.

C. Q_{max} derived from stimulus-recruitment data.

D. Q_{max} derived from interpulse time-recruitment data.

E. MCV.

Data are represented as mean ± sd. (*) Different compared to control nerves. (#) Different compared to autograft nerves.

The stimulus-recruitment curves (fig. 6A), corresponding to the figures representing the monophasic action currents (fig. 5A), demonstrated that the contribution of the Aα-fibres to Q_{max} was larger than the contribution of the Aβ-fibres, as in control and autografted nerves (fig. 6B).

The mean voltage threshold (V_{50}) was higher in grafted nerves in comparison to control nerves (fig. 6C), and the values of both $V_{50,\alpha}$ and $V_{50,\beta}$ doubled in all regenerating nerves (fig. 6D). In all regenerating nerves, the mean threshold voltage of the Aα-fibres ($V_{50,\alpha}$) was approximately half the value of $V_{50,\beta}$, in agreement with the values in the control nerves.

The interpulse time-recruitment curves, corresponding to those nerves of which the stimulus-recruitment curves were depicted in figure 6A, demonstrated again that the contribution

Figure 6: Stimulus-recruitment curves

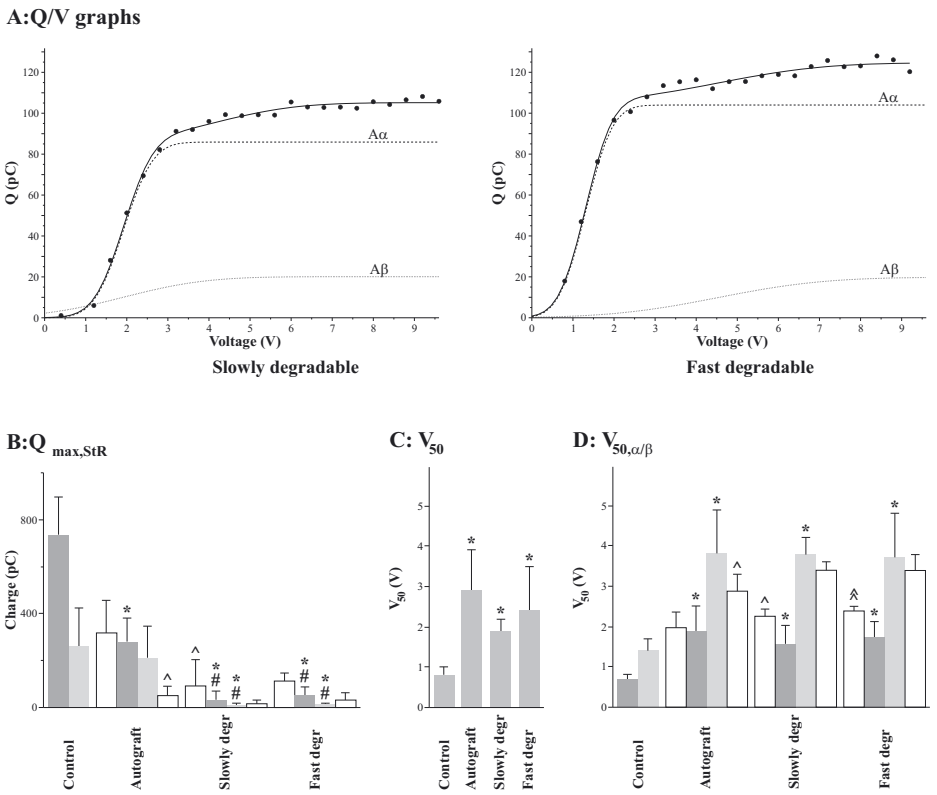

Solid circles represent data points. Continuous lines represent the fitted curves. In case the values for the Aα- and Aβ-fibres were very much alike, it was not in all electrophysiologically responding nerves possible to fit the sum of two *erf*-functions to the data. To still obtain an extrapolated value for $Q_{max,\alpha}$ and $Q_{max,\beta}$ for those nerves, the mean percentual contributions of the Aα- and Aβ-fibres to Q_{max} obtained in that group were applied to the implicated Q_{max}. If it concerned $Q_{max,\alpha}$ and $Q_{max,\beta}$ obtained from the stimulus-recruitment curve, values for $V_{50,\alpha}$ and $V_{50,\beta}$ were not obtained in those nerves. The AIC proved to be smaller ($p<10^{4}$) for two populations compared to one. B. The $Q_{max,\alpha}$ (black) and $Q_{max,\beta}$ (white) of control, autografted,*slowly degradable* and *fast degradable* grafted nerves derived from the stimulus-recruitment data. The predicted values of $Q_{max,\alpha}$ and $Q_{max,\beta}$ are represented by unfilled bars. C. Mean voltage threshold (V_{50}) of control, autografted, and synthetic grafted sciatic nerves. D. Mean firing threshold for the Aα- and Aβ-fibres separately ($V_{50,\alpha}$ and $V_{50,\beta}$) of control, autografted, and synthetic grafted sciatic nerves. The predicted values of $V_{50,\alpha}$ and $V_{50,\beta}$ are represented by unfilled bars. Data are represented as mean (± sd). (*) Different compared to control group. (#) Different compared to autograft group. (^) Different compared to predicted values, $p<0.05$. (^^) Different compared to predicted values, $p<0.10$.

of the Aα-fibres to Q_{max} was larger than the contribution of the Aβ-fibres (fig. 7A), as in control and autografted nerves (fig 7B).

The response in the auto- and*slowly degradable* grafted nerves was characterized by a longer mean refractory period (t_{50}) compared to control nerves (fig. 7C). In the *fast degradable* grafted nerves, t_{50} was comparable to control nerves. The mean refractory period of the Aα-fibres ($t_{50,\alpha}$) was approximately one third of $t_{50,\beta}$, both in control and in grafted nerves (fig. 7D). The value of $t_{50,\alpha}$ doubled in *slowly degradable* grafted nerves, but remained equal in autografted and *fast*

Figure 7: Interpulse time-recruitment curves

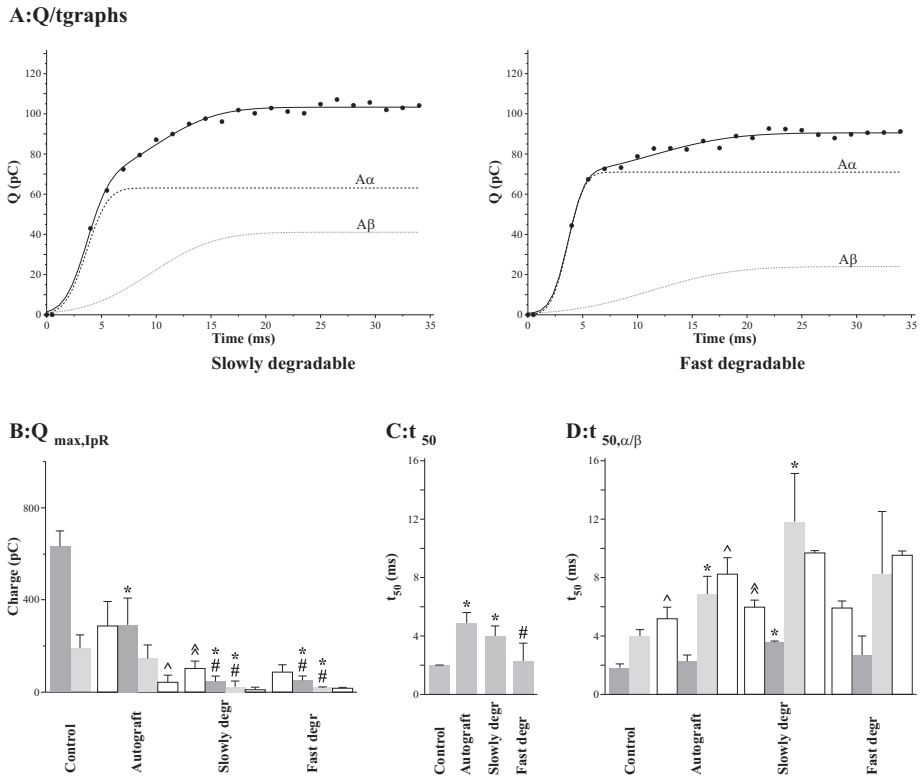

A: Interpulse time-recruitment graphs corresponding to the examples depicted in figure 5A. Solid circles represent data points. Continuous lines represent the fitted curves. The theoretical dataset ($\Delta t = 0$, $Q = 0$) was added to the data. The duration of the action current was sometimes so long that it (almost) equalled the interpulse timeinterval. In that case, no relevant curve could be obtained, and thus no value for Q_{max} could be obtained from the interpulse time-recruitment curve. In case the values for the Aα- and Aβ-fibres were very much alike, it was not in all electrophysiologically responding nerves possible to fit the sum of two *erf*-functions to the data. To still obtain an extrapolated value for $Q_{max,\alpha}$ and $Q_{max,\beta}$ for those nerves, the mean percentual contributions of the Aα- and Aβ-fibres to Q_{max} obtained in that group were applied to the implicated Q_{max}. If it concerned $Q_{max,\alpha}$ and $Q_{max,\beta}$ obtained from the interpulse time-recruitment curve, values for $t_{50,\alpha}$ and $t_{50,\beta}$ were not obtained in those nerves. The AIC proved to be smaller ($p<10^{-4}$) for two populations compared to one. B. The $Q_{max,\alpha}$ (black) and $Q_{max,\beta}$ (white) of control, autografted, *slowly degradable* and *fast degradable* grafted nerves derived from the interpulse time-recruitment data. The predicted values of $Q_{max,\alpha}$ and $Q_{max,\beta}$ are represented by unfilled bars. C. Mean refractory period (t_{50}) of control, autografted, and synthetic grafted sciatic nerves. D. Mean refractory period for the Aα- and Aβ-fibres separately ($t_{50,\alpha}$ and $t_{50,\beta}$) of control, autografted, and synthetic grafted sciatic nerves. The predicted values of $t_{50,\alpha}$ and $t_{50,\beta}$ are represented by unfilled bars. Data are represented as mean (± sd). (*) Different compared to control group. (#) Different compared to autograft group. ($) Different compared to *fast degradable* and *slowly degradable* group. (^) Different compared to predicted values, $p<0.05$. (^^) Different compared to predicted values, $p<0.10$.

degradable grafted nerves. The value of $t_{50,\beta}$ increased in the autografted and *slowly degradable* graft group, but remained unchanged in the *fast degradable* graft group.

Relation of morphometric and electrophysiological data

The measured V_{50} in the Aα-fibres was lower than predicted, both in the *slow* and *fast degradable* graft groups (fig. 8A). In the *slowly degradable* nerve graft group, the measured t_{50} in the

Figure 8: Observed and predicted values

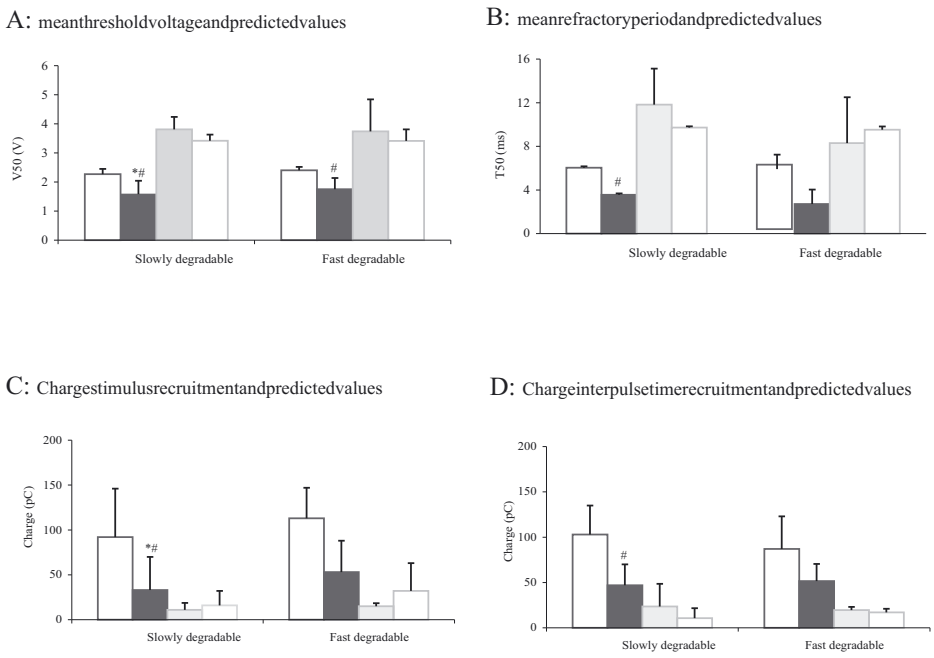

The measured values of V_{50} of the Aα-fibres (dark grey) and the Aβ-fibres (light grey) are compared with their predicted values (white). Data are represented as mean (± sd). (*) Different compared to predicted values, $p<0.05$. (#) Different compared to predicted values, $p<0.10$.

Aα-fibres was also lower than predicted (fig. 8B). In the *fast degradable* nerve graft group however, the measured t_{50} in the Aα- and in the Aβ-fibres could not statistically be discerned from predicted values. In the Aβ-fibres, the measured V_{50} and t_{50} were according to predictions.

In *slowly degradable* nerve grafted nerves, the measured charge in the Aα-fibres was lower than predicted, while in *fast degradable* nerve grafted nerves the measured charge was according to predictions. Both in *slow* and *fast degradable* nerve grafted nerves, the measured charge in the Aβ-fibres was just as was expected based on morphological changes.

Discussion

The influence of biodegradation of a synthetic nerve graft on peripheral nerve regeneration was investigated and it was demonstrated that the *fast degradable* graft actually desintegrated within twelve weeks while the *slowly degradable* graft remained partially intact. We observed subtle differences in electrophysiological properties between the two kinds of synthetic grafted nerves, and demonstrated that nerve fibres were positively influenced by faster degradation of the synthetic nerve graft.

Twelve weeks after surgery, the morphometrical parameters of the peroneal nerves and the gastrocnemic and tibial muscles were similar if not equal in both experimental groups. Electrophysiologically, however, there was a difference. The refractory periods of the Aα- and Aβ- fibres in the *fast degradable* nerve grafts were comparable to unoperated nerves, in contrast to the refractory periods in *slowly degradable* nerve grafts, that were longer. Based on this outcome *fast degradable* nerve grafts are preferred over *slowly degradable* nerve grafts because a shorter refractory period enables the axon to follow the firing frequency of the neuron more effectively. This allows a more adequate target organ stimulation.

To interpret the observed changes in electrophysiological parameters of both *fast* and *slowly degradable* nerve grafts, we compared the measured values to predicted values (see Materials and Methods). Equality of the measured and predicted values would indicate that no other changes but changes of diameter (and number) had occurred. Inequality would indicate that changes of other factors that influence these parameters must have played a role as well, like for instance shorter internodal distances, membrane composition, changes in transport mechanisms, and adjustments in the ion channel composition. The most obvious and best documented of such factors are changes in the expression of ion channels at or near the Ranvier nodes [44-48]. Apart from the conclusion that the expression of ion channels has probably changed, the direction of the change can also be qualified as compensation, overcompensation or decompensation (fig. 9). Should the observed value of an electrophysiological parameter fall between control and predicted values, this could be interpreted as meaning that the nerve fibres behave more like normal than expected, i.e. that some kind of compensation has occurred to offset changes of nerve fibre diameter (and number), indicated as **compensation**. Along similar lines of reasoning observed values beyond the predicted

Figure 9: Interpretation

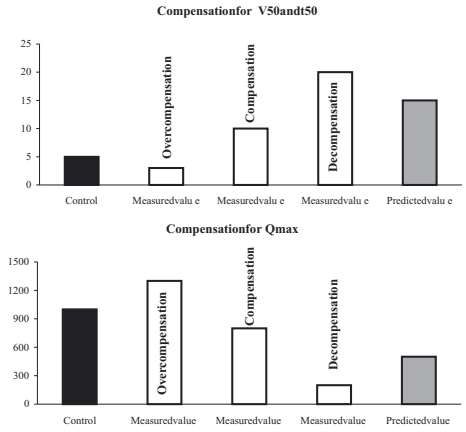

Should the observed value of an electrophysiological parameter fall between control and expected values, this could be interpreted as meaning that the nerve fibres behave more like normal than expected, i.e. that some kind of compensation has occurred to offset changes of nerve fibre diameter (and number), indicated as **compensation**. Along similar lines of reasoning observed values beyond the expected values would signify **decompensation**, and observed values beyond the normal value **overcompensation**.

values would signify **decompensation**, and observed values beyond the normal value **over-compensation**.

Considering the mean refractory periods it is demonstrated that in the Aα-fibres of the *slowly degradable* grafts the refractory period was even shorter than predicted, hinting at compensatory changes of the ion channel composition. However, it is very likely that these same compensatory mechanisms were present in the fast degradable nerve grafts, although they could not be demonstrated to be statistically significant. A compensatory mechanism leading to a shorter refractory period would be the upregulation of the $Na_{v1.3}$ channels [45, 49]. A shorter refractory period could also be caused by a faster potassium efflux, which can be effectuated by an increase in the number of channels in the membrane or by more effective closing of the channels [50].

The mean voltage thresholds increased in all grafted nerves. In the Aα-fibres of both the *fast* and *slowly degradable* nerve grafts the measured mean voltage thresholds were lower than predicted (fig. 8A), indicating possible compensation. This could be due to a more positive resting membrane potential.

The conducted charge decreased in both *fast* and *slowly degradable* nerve grafts, but in *slowly degradable* grafts this decrease was even larger than predicted, thus the nerve fibers in these grafts performed worse than was to be expected. It is possible that not all the nerve fibres present in the *slowly degradable* nerve grafts contributed to the displacement of charge. This might be due to non-functioning of the voltage gated sodium channels, which may prevent the axon from depolarising [53], but it is also possible that a number of the nerve fibers were degenerating, and incapable of conduction. So with respect to the charge conducting capacity the *fast degradable* graft are (again) preferred over the *slowly degradable* grafts.

The effects of porosity and biodegradability are not always easy to distinguish [10], especially since biodegradation by itself will change the permeability of a synthetic nerve graft. To reduce the potential effect of porosity in the present study the synthetic nerve grafts that we compared in this study were both microporous to start with. Theoretically, however, it is possible that the different degradation speeds of the two nerve guides under comparison might influence their pore size differently. As pore size can increase with progressive degradation the pores may enlarge faster in the *fast degradable* graft. This may ultimately lead to the inward migration of fibroblasts, resulting in the overgrowth of collageneous tissue in the graft [chapter 4 this thesis, 51]. We did not observe this overgrowth in the *fast degradable* nerve grafts. Apparently the potential detrimental effect of large pores in the early phase of regeneration is dependent upon the continuous presence of a surrounding tubal wall, which might act as a scaffold for the formation of collagenous scar tissue. This, in turn, attests to the interrelation of porosity and degradability.

In theory a degradable graft is better than a non degradable one, because upon growth of the nerve cable its diameter will increase, and the nerve cable may become physically constricted by the graft. Compression will compromise the microvascular supply of the nerve fibres, causing local ischemia [54 for review]. This will result in conduction block [55], which

can completely or partially impair fast [56] and slow [57] anterograde and retrograde [54 for review] transport of growth factors. However, should the graft disappear in time, compression would only be exerted temporarily, and presumably be less severe during the degradation process.

Regenerating nerve fibres may also be negatively influenced by a foreign body response towards the implanted graft [58]. The accompanying inflammatory edema in and around the graft will also compress the regenerating nerve fibres. Moreover, inflammatory products like cytokines may have a deleterious effect on the newly regenerated nerve fibres [59-61] and on the Schwann cells [62]. Should the graft degrade quickly then the putative foreign body response would be only temporary.

The detrimental effects of peripheral nerve axotomy ultimately depend on alterations in the expression of neuropeptides and their receptors, which involve the downregulation of excitatory peptides (like substance P) and the upregulation of inhibitory peptides (like pituitary adenylate cyclase-activating polypeptide (PACAP), resulting in a reduction of transmission [63]. These same processes play a role in compression on an inflammation of the peripheral nerve fibres, though it is likely that these changes are far more pronounced in nerve transection than in the less injurious processes of nerve compression or inflammation. It was indeed demonstrated that PACAP dramatically upregulated after axotomy in medium-large neurons, but only moderately after inflammation [64]. Activating transcription factor 3 (ATF3) plays a crucial role in stressed tissue by upregulating in sensory and motoneurons after nerve transections [65] or compression [66], as does c-Jun which is related to successful regenerative nerve growth [67]. Inevitably study of the effect of graft biodegradability on nerve regeneration involves nerve transection. Transection and compression/inflammation result in the same effect, but the small effect of compression/inflammation is superimposed on the large effect of transection. Hence it is hardly surprising that the beneficial effect of graft biodegradation is difficult to resolve.

Nevertheless it was demonstrated that in *fast degradable* nerve guides the mean refractory period was short and the charge conducted conform predictions as opposed to an increased refractory period and a lower than predicted conducted charge in *slowly degradable* nerve guides. This indicated a subtle but decisive beneficial effect of graft biodegradation on nerve fibre electrophysiological properties in the early phase of regeneration. The observation that the properties of a synthetic nerve guide can indeed influence the electrophysiological properties of the regenerating nerve fibres is noteworthy. Moreover, the structural design of the regenerated nerve in its final appearance is established in this early phase of regeneration and the factors that influence this should be considered as very important.

References

1. Barrows T. Degradable implant materials: a review of synthetic absorbable polymers and their applications. Clinical Materials 1986;1:233-257.
2. Fields RD, Beau le JM, Longo LM, Ellisman MH. Nerve regeneration through artificial tubular im - plants. Brogress in Neurobiology 1989;33:87-134.
3. Danielsen N. Regeneration of the rat sciatic nerve in the silicone chamber model. Restorative Neurology and Neuroscience 1990;1:253-259.
4. Fawcett JW, Keynes RJ. Peripheral nerve regeneration. Annu. Rev. Neurosci 1990;13:43-60.
5. Brunelli GA, Vigasio A, Brunelli GR. Different conduits in peripheral nerve surgery. Microsurgery 1994;15:176-8.
6. Doolabh VB, Hertl MC, Mackinnon SE. The role of conduits in nerve repair: a review. Reviews in the Neurosciences 1996;7:47-84.
7. Heath CA, Rutkowski GE. The development of bioartificial nerve grafts for peripheral-nerve regen - eration. Trends Biotechnol 1998;16:163-8.
8. Strauch B. Use of nerve conduits in peripheral nerve repair. Hand Clin 2000;16:123-30.
9. Dahlin LB, Lundborg G. Use of tubes in peripheral nerve repair. Neurosurg Clin N Am 2001;12:341-52.
10. Rodriguez FJ, Gomez N, Perego G, Navarro X. Highly permeable polylactide-caprolactone nerve guides enhance peripheral nerve regeneration through long gaps. Biomaterials 1999;20:1489-500.
11. Chamberlain LJ, Yannas IV, Hsu HP, Strichartz G, Spector M. Collagen-GAG substrate enhances the quality of nerve regeneration through collagen tubes up to level of autograft. Exp Neurol 1998;15:315-329.
12. Valero-Cabre A, Tsironis K, Skouras E, Perego G, Navarro X, Neiss WF. Superior muscle reinnervation after autologous nerve graft or poly-L-lactide-epsilon-caprolactone (PLC) tube implantation in comparison to silicone tube repair. J. Neurosci, Res 2001;63:214-223.
13. Wang S, Wan AC, Xu X, Gao S, Mao HQ, Leong KW, Yu H. A new nerve guide conduit material composed of a biodegradable poly(phosphoester). Biomaterials 2001;22:1157-1169.
14. Navarro X, Rodriguez FJ, Labrador RO, Buti M, Ceballos D, Gomez N, Cuadras J, Perego G. Periph - eral nerve regeneration through bioresorbable and dura ble nerve guides. J. Peripher. Nerv. Sys. 1996;1:53-64.
15. Favaro G, Bortolami C, Cereser S, Dona M, Pastorello A, Callegaro L, Fiori MG. Peripheral nerve re - generation through a novel bioresorbable nerve guide. Trans Am Soc Artif Intern Organs 1990;36: M291-M294.
16. Mohammad J, Shenaq J, Rabinovsky E, Shenaq S. Modulation of peripheral nerve regeneration: a tissue-engineering approach. The role of amnion tube nerve conduit across a 1-centimeter nerve gap. Plast Reconstr Surg 2000;105:660-666.
17. Madison RD, da Silva C, Dikkes P, Sidman RL, Chiu TH. Peripheral nerve regeneration with entu - bulation repair: comparison of biodegradable nerve guides versus polyethylene tubes and the effects of a laminin-containing gel. Experimental neurology 1987;95:378-390.
18. Harley BA, Spilker MH, Wu JW, Asano K, Hsu HP, Spector M, Yannas IV. Optimal degradation rate for collagen chambers used for regeneration of peripheral nerves over long gaps. Cells Tissues Organs 2004;176:153-165.
19. Seckel BR, Chiu TH, Nyilas E, Sidman RL. Nerve regeneration through synthetic biodegradable nerve guides: regulation by the target organ. Plast Reconstr Surg 1984;74:173-181.

20. Vleggeert-Lankamp CLAM, Van den Berg RJ, Feirabend HKP, Lakke EAJF, Malessy MJA, Thomeer RTWM. Electrophysiology and morphometry of the Aalpha and Abeta fibre populations in the normal and regenerating rat sciatic nerve. Experimental Neurology 2004;187:337-349.
21. Vleggeert-Lankamp CLAM, Ruiter de GCW, Wolfs JFC, Pego AP, Feirabend HKP, Lakke EAJF, Malessy MJA. Type grouping in skeletal muscles after experimental reinnervation: another explanation. European Journal of Neuroscience 2005;21:1249-1256.
22. MacKinnon SE, Dellon AL. A study of nerve regeneration across synthetic (Maxon) and bio logic (collagen) nerve conduits for nerve gaps up to 5 cm in the primate. J Reconstr Microsurg 1989;6:117-121.
23. Keeley R, Atagi T, Sabelman E, Padilla J, Kadlcik S, Keeley A, Nguyen K, Rosen J. Peripheral nerve regeneration across 14-mm gaps: a comparison of autograft and entubulation repair methods in the rat. J Reconstr. Microsurg. 1993;9:349-358.
24. Rosen JM, Padilla JA, Nguyen KD, Siedman J, Pha HN. Artificial nerve graft using glycolide trimeth ylene carbonate as a nerve conduit filled with collagen compared to sutured autograft in a rat model. Journal of Rehabilitation Research 1992;29:1-12.
25. Lietz M, Ullricht A, Schulte-Eversum C, Oberhoffner S, Fricke C, Muller HW, Schlosshauer B. Physical and biological performance of a novel block copolymer nerve guide. Biotechnology and bioengi neering 2005.
26. Katz AR, Mukherjee DP, Kaganov AL, Gordon S. A new synthetic monofilament absorbable suture made from polytrimethylene carbonate. Surg Gynecol Obstet 1985;161:213-222.
27. Pitt CG. Poly-e-caprolactone and its copolymers. In: Chasin M, Langer R, eds. Biodegradable poly mers as drug delivery system. New York: Marcel Dekker, 1990:71-120.
28. Pego AP, Poot AA, Grijpma DW, Feijen J. Copolymers of trimethylene carbonate and epsilon-cap rolactone for porous nerve guides: synthesis and properties. J Biomater Sci Polym Ed 2001;12:35-53.
29. Pitt CG, Chasalow FI, Hibionada DM, Klimas DM, Schindler A. Aliphatic polyesters. I. The degrada tion of poly(e-caprolactone) in vivo. J Appl Polym Sci 1981;26:3779=3787.
30. Pego AP, Poot AA, Grijpma DW, Feijen J. Biodegradable elastomeric scaffolds for soft tissue engi neering. J Control Release 2003;87:69-79.
31. Pego AP, Poot AA, Grijpma DW, Feijen J. Biodegradable elastomeric scaffolds for tissue engineer ing. Proceedings of the 4th international symposium on frontiers in biomedical polymers. Wil liamsburg, Virginia, USA, 2001:54.
32. Pego AP. Biodegradable polymers based on trimethylene carbonate for tissue engineering ap plications. Polymer Chemistry and Biomaterials. Enschede: University of Twente, 2002:291.
33. Marani E. A method for orienting cryostat sections for three-dimensional reconstructions. Stain Technol. 1978;53:265-268.
34. Kluver H, Barrera E. A method for the combined staining of cells and fibers in the nervous system. Neuropath Exp Neur 1953;12:400-403.
35. Bancroft JD, Gamble M. Theory and practice of histological techniques. London: Churchill Living stone, 2002.
36. Feirabend HKP, Choufoer H, Ploeger S. Preservation and staining of myelinated nerve fibers. Meth ods 1998;15:123-31.
37. Blair EA, Erlanger J. A comparison of the characteristics of axons through their individual electrical responses. Am J Physiol 1933;106:524-564.
38. Jack JJB, Noble D, Tsien RW. Electric current flow in excitable cells: Oxford University Press, 1983.
39. Paintal AS. The influence of diameter of medullated nerve fibres of cats on the rising and falling phases of the spike and its recovery. J Physiol 1966;184:791-811.

40. Rushton WAH. A theory of the effects of fiber size in medullated nerve. J Physiology 1951;115:101-122.
41. Kolmogorov A. Confidence limits for an unknown distribution function. Ann. Meth. Statist. 1941;12:461-463.
42. Smirnow NV. Table for estimating the goodness of fit of empirical distributions. Ann. Meth. Statist. 1948;19:279-281.
43. MacKinnon SE, Hudson AR, Hunter DA. Histologic assessment of nerve regeneration in the rat. Plast Reconstr Surg 1985;75:384-388.
44. Querfurth HW, Armstrong R, Herndon RM. Sodium channels in normal and regenerated feline ventral spinal roots. J Neurosci 1987;7:1705-1716.
45. Cummins TR, Waxman SG. Downregulation of tetrodotoxin-resistant sodium currents and up - regulation of a rapidly repriming tetrodotoxin-sensitive sodium current in small spinal sensory neurons after nerve injury. J Neurosci 1997;17:3503-14.
46. Everill B, Kocsis JD. Reduction in potassium currents in identified cutaneous afferent dorsal root ganglion neurons after axotomy. J Neurophysiol 1999;82:700-8.
47. Baccei ML, Kocsis JD. Voltage-gated calcium currents in axotomized adult rat cutaneous afferent neurons. J Neurophysiol 2000;83:2227-38.
48. Lancaster E, Weinreich D. Sodium currents in vagotomized primary afferent neurones of the rat. J Physiol 2001;536:445-458.
49. Waxman SG. Transcriptional channelopathies: an emerging class of disorders. Nat Rev Neurosci 2001;2:652-9.
50. Yellen G. The voltage-gated potassium channels and their relatives. Nature 2002;419:35-42.
51. O'Brien FJ, Harley BA, Yannas IV, Gibson LJ. The effect of pore-size on cell adhesion in collagen-GAG scaffolds. Biomaterials 2005: 26; 433-441.
52. Waxman SG, Cummins TR, Black JA, Dib-Hajj S. Diverse functions and dynamic expression of neuronal sodium channels. Novartis Found Symposium, 2002:34-51, discussion 51-60.
53. Goldin AL. Evolution of voltage-gated Na+ channels. J Exp Biol 2002;205:575-584.
54. Lundborg G, Dahlin LB. The pathophysiology of nerve compression. Hand Clinics 1992;8:215-227.
55. Lundborg G, Gelberman RH, Minteer-Convery M. Median nerve compression in the carpal tunnel - functional response to experimentally induced controlled pressure. J Hand Surg 1992;7:252.
56. Rydevik B, McLean WG, Sjostrand J. Blockage of axonal transport induced by actute, graded com - pression of the rabbit vagus nerve. J Neurol Neurosurg Psychiatry 1981;43:690.
57. Dahlin LB, W.G. M. Effects of graded experimental compression on slow and fast axonal tranport in rabbit vagus nerve. J Neurol Sci 1986;72:19.
58. Den Dunnen WF, Van der Lei B, Schakenraad JM, Blaauw EH, Stokroos I, Pennings AJ, Robinson PH. Long-term evaluation of nerve regeneration in a biodegradable nerve guide. Microsurgery 1993;14:508-515.
59. Creange A, Barlovatz-Meimon G, Gherardi RK. Cytokines and peripheral nerve disorders. Eur Cytokine Netw 1997;8:145-51.
60. Wu LC, Goettl VM, Madiai F, Hackshaw KV, Hussain SR. Reciprocal regulation of nuclear factor kappa B and its inhibitor ZAS3 after peripheral nerve injury. BMC Neurosci 2006;7:4.
61. Sommer C, Kress M. Recent findins on how proinflammatory cytokines cause pain: peripheral mechnaisms in inflammatory and neuropathic hyperalgesia. Neuroci Lett 2004;361:184-187.
62. Oliveira RB, Sampaio EP, Aarestrup F, Teles RM, Silva TP, Oliveira AL, Antas PR, Sarno EN. Cytokines and Mycobacterium leprae induce apoptosis in human Schwann cells. J Neuropathol Exp Neurol 2005;64:882-890.

63. Hokfelt T, Zhang X, Wiesenfeld-Hallin Z. Messenger plasticity in primary sensory neurons following axotomy and its functional implications. Trends Neurosci 1994;17:22-30.
64. Pettersson LME, Dahlin LB, Danielsen N. Changes in expression of PACAP in rat sensory neurons in response to sciatic nerve compression. Eur J Neurosci 2004;20:1838-1848.
65. Tsujino H, Kondo E, Fukuoka T, Dai Y, Tokunaga A, Miki K, Yonenobu K, Ochi T, Noguchi K. Activating transcription factor 3 (ATF3) induction by axotomy in sensory and motoneurons: a novel neuronal marker of nerve injury. Molecular and Cellular Neuroscience 2000;15:170-182.
66. Isacsson A, Kanje M, Dahlin LB. Induction of activating transcription factor 3 (ATF3) by peripheral nerve compression. Scand J Plast Reconstr Hand Surg 2005;39:65-72.
67. Broude E, McAtee M, Kelley MS, Bregman BS. c-Jun expression in adult rat dorsal root ganglion neurons: differential response after central or peripheral axotomy. Exp Neurol 1997;148:367-377.
68. Krarup C, Horowitz SH, Dahl K. The influence of the stimulus on normal sural nerve conduction velocity: a study of the latency of activation. Muscle Nerve 1992;15:813-21.